Carbon Capture from Natural Gas Flue Emissions and Air via (Bi)Carbonate Formation in a Cyclodextrin-Based Metal-Organic Framework

S. Alexandra Lim,[a,‡] Mary E. Zick,[a,‡,†] Jaehwan Kim,[a,§] Benjamin J. Rhodes,[b] Tristan A. Pitt,[a] Ronald T. Jerozal,[a,¶] Alexander C. Forse,[b] Phillip J. Milner[a,*]

[a]Department of Chemistry and Chemical Biology, Cornell University, Ithaca, NY, 14850, United States

[b]Department of Chemistry, University of Cambridge, Cambridge, CB2 1EW, United Kingdom

ABSTRACT: Carbon capture and utilization or sequestration (CCUS) from industrial point sources and direct air capture (DAC) are both necessary to curb the rising atmospheric levels of CO_2. Amine scrubbers, the current leading carbon capture technology, suffer from poor oxidative and thermal stability, limiting their long-term cycling stability under oxygen-rich streams such as air and the emissions from natural gas combined cycle (NGCC) power plants. Herein, we demonstrate that the hydroxide-based cyclodextrin metal-organic framework (CD-MOF) Rb_2CO_3 CD-MOF ST possesses high CO_2 capacities from dry dilute streams at low temperatures and humid streams at elevated temperatures. Additionally, it displays good thermal, oxidative, and cycling stabilities and selective CO_2 capture under mixed gas conditions in dynamic breakthrough experiments. Unexpectedly, under dry, hot conditions, a shift in the CO_2 adsorption mechanism—from reversibly formed bicarbonate to irreversibly formed carbonate—is observed, as supported by gas sorption and spectroscopic studies. This mechanistic switch, akin to urea formation in amine-functionalized sorbents, has not been previously reported in a hydroxide-based material and sheds new light on the interplay between bicarbonate and carbonate species during CO_2 capture. Our findings provide valuable insight for the design of next-generation materials containing oxygen-based nucleophiles for carbon capture applications.

Introduction.

One of the greatest challenges facing humankind is climate change resulting from the rising atmospheric levels of CO_2.[1,2] Because we cannot switch over to low-emission energy sources quickly enough, carbon capture and utilization or sequestration (CCUS), in which CO_2 is selectively removed from the emissions of fossil fuel-fired power plants, will be required to mitigate the rise in average global temperature over the next century.[3,4] Global emissions from the combustion of natural gas for energy production are on track to surpass those from coal over the next decade, as they already have in the United States, making them a good target for future CCUS technologies.[5] Further, to address legacy emissions, direct air capture (DAC)—the use of sorbents to remove CO_2 from the atmosphere—will likely also be necessary.[1,6–9] Current approaches for CCUS and DAC are likely too expensive for broad deployment without significant subsidies, necessitating the development of more efficient carbon capture technologies.[4]

Removing CO_2 from the flue gas of natural gas combined cycle (NGCC) power plants (30–50 mbar CO_2, 750 mbar N_2, 100–120 mbar O_2, 11–100% relative humidity, 40–100 °C) and from air (0.42 mbar CO_2, 780 mbar N_2, 210 mbar O_2, 0–100% relative humidity) presents similar challenges.[10,11] The primary thermodynamic barrier for carbon capture from either stream is the low partial pressure of CO_2.[12,13] Most sorbents cannot bind CO_2 efficiently at such low partial pressures, and those that can require high temperatures (>120 °C) to release CO_2, leading to large energetic penalties and decomposition upon cycling.[14,15] Another shared challenge is the high O_2 content of both streams, which contributes to the oxidative degradation of many sorbents, such as amines.[16–27] Competitive co-adsorption of H_2O over CO_2 is also a limitation for sorbents such as zeolites.[28] Owing to these challenges, effective sorbents for carbon capture from NGCC emissions and air remain relatively rare.

The two leading technologies for carbon capture are (i) amine-based sorbents, including aqueous amine solutions[29] and amine-functionalized porous solids,[30–33] and (ii) aqueous hydroxide (OH^-) solutions.[34,35] Amine-based sorbents operate through the selective reaction with CO_2 to form ammonium carbamates, bicarbonates (HCO_3^-), and/or carbonates (CO_3^{2-}). Although well-studied for a range of carbon capture processes, most amine-based sorbents are plagued by oxidative degradation.[16–27] For example, the commercial polymer Lewatit R VP OC 1065 used for DAC undergoes significant decomposition upon heating in air.[18,19,25] Aqueous OH^- solutions have emerged as promising alternatives for DAC due to their stability and high affinity for CO_2 via (bi)carbonate formation.[34,35] The main limitations of these systems are the high temperatures (>800 °C) and large amounts of energy (>5 GJ/ton CO_2) required for CO_2 release from the corresponding (bi)carbonate salts.[36–39] For example, $CaCO_3$ must be heated to >800 °C to release CO_2 and regenerate active CaO in a calcium-looping process.[34,35] Related OH^--rich anion exchange membranes suffer from slow kinetics and low capacities.[40,41] New OH^--based sorbents that maintain the excellent oxidative stability and CO_2 capture selectivity of OH^- salts but with lower regeneration costs, faster kinetics, and better performance under humid conditions would be cutting edge materials for carbon capture from dilute streams.

Recently, we[42] and others[43–54] have shown that isolating reactive OH^- sites within porous metal-organic frameworks (MOFs) produces materials with high CO_2 affinities, which are generally proposed to operate via reversible HCO_3^- formation. Among these, only $Zn_5(OH)_4(bibta)_3$ ($bibta^{2-}$ = 5,5′-bibenzotriazolate) and closely related materials have been definitively shown to

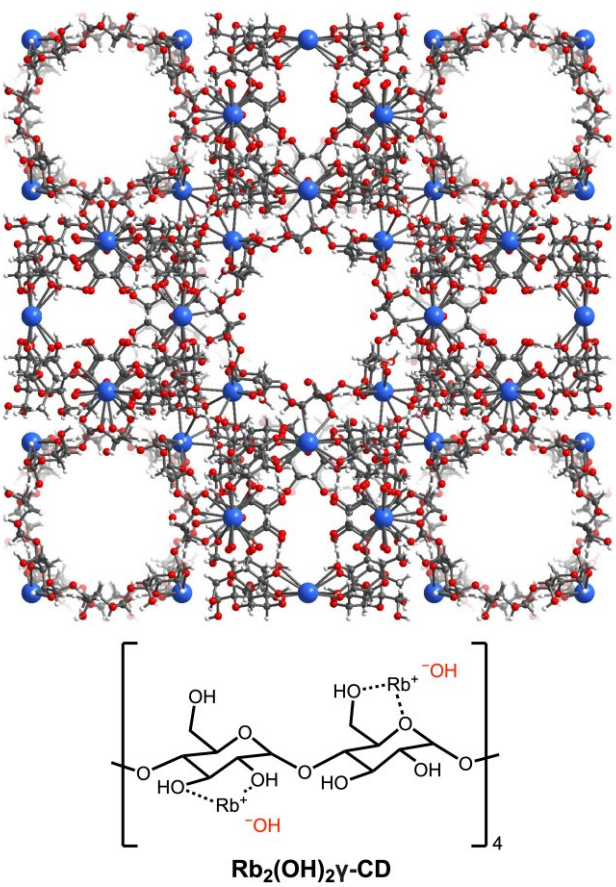

Figure 1. Structure of cubic CD-MOF-2.[58] Blue, red, grey, and white spheres correspond to rubidium, oxygen, carbon, and hydrogen atoms, respectively. The charge-balancing OH^- sites that participate in CO_2 capture are disordered, so they have been omitted in this figure.

facilitate DAC under dry conditions.[47] Unfortunately, most of these materials, including $Zn_5(OH)_4(bibta)_3$, do not capture CO_2 under humid conditions.[42,47] One potential avenue to address this challenge would be to carry out carbon capture at elevated temperatures (>100 °C), which has recently gained interest to avoid unnecessary cooling of flue gas.[55] However, the use of OH^--rich porous solids for high-temperature CO_2 capture has not been demonstrated to date.

Herein, we establish a new solvothermal method to prepare the framework Rb_2CO_3 CD-MOF (CD = cyclodextrin) from Rb_2CO_3 (referred to herein as Rb_2CO_3 CD-MOF ST). This MOF possesses high CO_2 uptake from dilute streams, including dry air (~0.7 mmol/g at 25 °C) and NGCC emissions (~1.4 mmol/g at 40 °C). In addition, Rb_2CO_3 CD-MOF ST displays similar or improved CO_2 capture performance under humid conditions at elevated temperatures (80–120 °C), a rare achievement for a OH^--based material. In exploring high-temperature CO_2 capture with Rb_2CO_3 CD-MOF ST under dry conditions, we also observed an unexpected shift in chemisorbed species from reversibly formed HCO_3^- to irreversibly formed CO_3^{2-}, as supported by diffuse reflectance infrared Fourier transform spectroscopy (DRIFTS) and solid-state nuclear magnetic resonance (SSNMR) measurements. This change in mechanism—akin to urea formation in amine-functionalized silicas[56]—has not been observed previously in a OH^--based sorbent and provides important insight into the role of HCO_3^- and CO_3^{2-} species upon CO_2 capture in these materials. Elucidating the mechanism of CO_2 capture in Rb_2CO_3 CD-MOF paves the way for the design of next-generation porous materials bearing nucleophilic OH^- sites for carbon removal from dry and humid streams. Additionally, our findings highlight that OH^--based materials are best suited for capture from dry dilute streams at low temperatures and humid streams at elevated temperatures.

Results and Discussion.

Our previous work demonstrated that the use of less basic precursors under ST conditions produces K-based CD-MOFs with improved gas sorption properties compared to those traditionally prepared from KOH via vapor diffusion (VD).[42] We also found that moving from harder K to softer Rb cations in cubic γ-cyclodextrin-based $M_2(OH)_2$(γ-CD) MOFs (Figure 1)[57] leads to stronger CO_2 binding, but the reported framework $Rb_2(OH)_2$(γ-CD) or CD-MOF-2 prepared via VD (referred to herein as RbOH CD-MOF VD)[58] exhibits poor thermal and mechanical stability, making it unsuitable for carbon capture applications.[42]

To better evaluate the suitability of Rb-based CD-MOFs for CO_2 capture from dilute streams, frameworks were prepared from RbOH and Rb_2CO_3 as precursors under both VD and ST conditions (see SI Section 2 for details).[42,59] The resulting frameworks—termed RbOH CD-MOF VD, RbOH CD-MOF ST, Rb_2CO_3 CD-MOF VD, and Rb_2CO_3 CD-MOF ST—were characterized by powder X-ray diffraction (PXRD) as well as scanning electron microscopy (SEM) and surface area analysis (see SI Section 2 for details). Pawley refinements of PXRD data confirm that RbOH CD-MOF VD (SI Figure S8), RbOH CD-MOF ST (SI Figure S16), and Rb_2CO_3 CD-MOF ST (SI Figure S2) form the CD-MOF-2 cubic phase (Figure 1).[58] Consistently, SEM revealed that both RbOH CD-MOF VD (SI Figure S10) and Rb_2CO_3 CD-MOF ST (SI Figure S6) crystallize as well-defined cubes, with RbOH CD-MOF VD forming as large mm-sized crystals and Rb_2CO_3 CD-MOF ST forming as smaller (~26 μm) crystals. In contrast, Rb_2CO_3 CD-MOF VD crystallizes as a distinct phase or mixture of phases that do(es) not match any reported CD-MOF (SI Figure S11). SEM shows that this material forms as rectangular plates instead of the desired cubes (SI Figure S12). The 77 K N_2 Brunauer–Emmett–Teller (BET) surface area of Rb_2CO_3 CD-MOF VD is also significantly lower (304 ± 1 m^2/g, SI Figure S13) than that of Rb_2CO_3 CD-MOF ST (1199 ± 12 m^2/g, SI Figure S3), highlighting the advantage of solvothermal methods for synthesizing high surface area CD-MOFs.[42]

The optimal activation temperature for each CD-MOF under flowing N_2 was systematically determined using thermogravimetric analysis (TGA) (SI Figures S31–S34). To measure CO_2 uptake capacities, pure CO_2 at atmospheric pressure and 30 °C was flowed over activated samples of all four frameworks (Figure 2a). Rb_2CO_3 CD-MOF ST exhibits a much higher CO_2 capacity (2.20 mmol/g) than Rb_2CO_3 CD-MOF VD (1.30 mmol/g). The poor performance of Rb_2CO_3 CD-MOF VD is presumably because it forms a less porous phase or mixture of phases. In addition, Rb_2CO_3 CD-MOF ST outperforms frameworks prepared from RbOH under both VD (1.48 mmol/g) and ST conditions (1.95 mmol/g). The superior uptake of Rb_2CO_3 CD-MOF ST compared to RbOH CD-MOF VD is likely because the latter forms as large, mechanically fragile crystals (SI Figure S10).

Beyond adsorption capacity, the long-term stability of adsorbents is a critical consideration for their application under realistic conditions. The oxidative and thermal stabilities of Rb_2CO_3

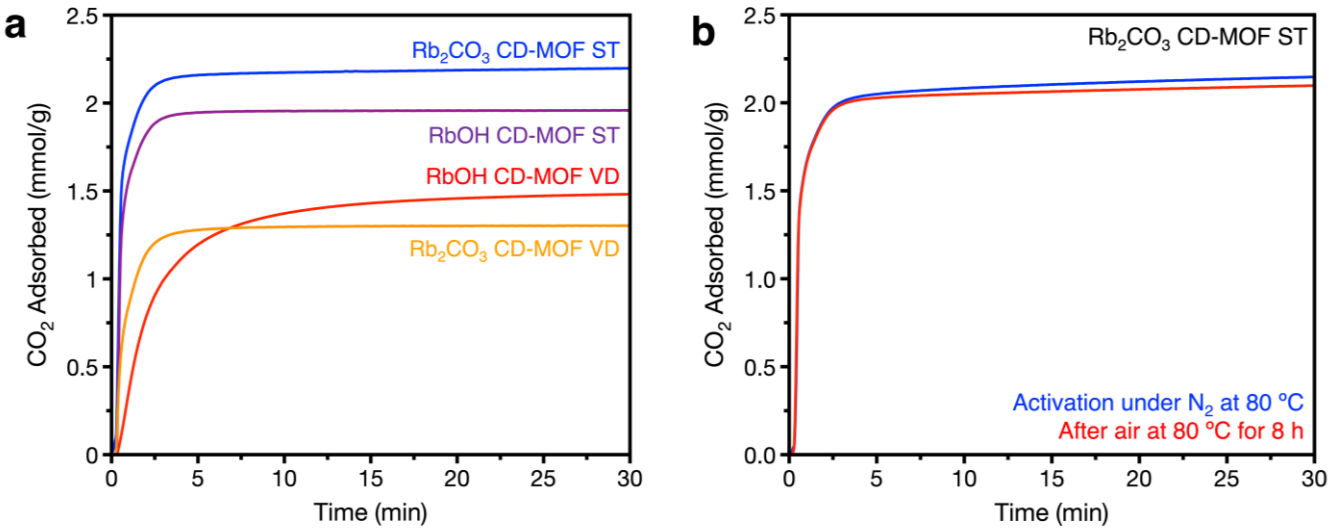

Figure 2. a) 30 °C pure CO_2 adsorption profiles of Rb_2CO_3 CD-MOF ST, RbOH CD-MOF ST, RbOH CD-MOF VD, and Rb_2CO_3 CD-MOF VD, as measured by TGA at a flow rate of 60 mL/min. The frameworks were activated under flowing N_2 for 30 min at 80 °C, 90 °C, 120 °C, and 70 °C, respectively. b) 30 °C pure CO_2 adsorption profiles of Rb_2CO_3 CD-MOF ST after activation under flowing N_2 for 30 min at 80 °C (blue) and after heating under flowing air at 80 °C for 8 h (red).

CD-MOF ST were evaluated by exposing it to flowing dry air (~21% O_2 in N_2) at different temperatures for 8 h, simulating hundreds of regeneration cycles (Figure 2b, SI Figure S30). Minimal changes were observed in the pure CO_2 adsorption profile after the extended treatment at 80 °C, confirming the stability of Rb_2CO_3 CD-MOF ST towards O_2 at moderately high temperatures. This finding supports that Rb_2CO_3 CD-MOF ST displays exceptional CO_2 uptake and thermal/oxidative stability among Rb-based CD-MOFs. As such, its promise for CO_2 capture from dilute streams was further evaluated (Figures 3–5).

To gain additional insight into the thermodynamics of CO_2 adsorption in Rb_2CO_3 CD-MOF ST, CO_2 adsorption (closed circles) and desorption (open circles) isotherms were collected at 25 °C, 40 °C, and 55 °C (Figure 3a–b). This material exhibits steep and reversible adsorption of CO_2 at low pressures, leading to good uptake from air (0.72 mmol/g at 0.40 mbar CO_2 and 25 °C) and NGCC flue gas (1.40 mmol/g at 50 mbar CO_2 and 40 °C) (Figure 3b). The adsorption isotherms were fit with dual-site Langmuir models (SI Tables S1–S3, see SI Section 3 for details). Using these fits, the heats ($-\Delta H_{ads}$), entropies ($-\Delta S_{ads}$), and free energies ($-\Delta G_{ads}$) of adsorption at 25 °C and 40 °C as a function of uptake for Rb_2CO_3 CD-MOF ST were determined using the Clausius-Clapeyron equation (Table S4, see SI Section 3 for details). Intriguingly, the $-\Delta H_{ads}$ trend for Rb_2CO_3 CD-MOF ST supports that the mechanism of CO_2 adsorption switches from chemisorption ($-\Delta H_{ads} \approx 64$ kJ/mol) to physisorption ($-\Delta H_{ads} \approx 20$ kJ/mol) at a loading of approximately 1 mol CO_2 per mol OH^-, assuming a molecular formula of $Rb_2(OH)_2$(γ-CD) (Figure 3c).[58] This finding is consistent with carbon capture via reversible HCO_3^- formation in this temperature range.[42]

Next, non-competitive CO_2/N_2 and CO_2/O_2 selectivities for Rb_2CO_3 CD-MOF ST were calculated using N_2 and O_2 isotherms measured at 25 °C, 40 °C, and 55 °C (Figure 3a, triangles and squares, respectively, SI Table S5). Fitting these isotherms to dual-site Langmuir models (SI Figures S24–S25, Tables S2–S4) confirms that Rb_2CO_3 CD-MOF ST exhibits minimal affinity towards both N_2 ($-\Delta H_{ads} = 9.6 \pm 1.8$ kJ/mol) and O_2 ($-\Delta H_{ads} = 3.1 \pm 2.2$ kJ/mol). Owing to the chemisorptive pathway for CO_2 adsorption, Rb_2CO_3 CD-MOF ST displays excellent non-competitive CO_2/N_2 and CO_2/O_2 selectivities. Under NGCC flue gas conditions (50 mbar CO_2, 120 mbar O_2, 750 mbar N_2, 40 °C), non-competitive CO_2/N_2 and CO_2/O_2 selectivities of 212 and 257, respectively, were calculated (SI Table S5). For DAC (0.4 mbar CO_2, 210 mbar O_2, 780 mbar N_2, 25 °C), Rb_2CO_3 CD-MOF ST exhibits exceptional non-competitive CO_2/N_2 and CO_2/O_2 selectivities of 11530 and 13875, respectively (SI Table S5).

The kinetics of CO_2 capture from dilute streams with Rb_2CO_3 CD-MOF ST were next evaluated via TGA (Figure 3d, see SI Section 4 for details). Promisingly, this framework captures 1.30 mmol/g of CO_2 from a 5% CO_2 in N_2 stream at 40 °C, with saturation reached in less than 2 min. Under 400 ppm CO_2 in air at 25 °C, 0.76 mmol/g of CO_2 was captured after 200 min, with saturation nearly reached after 100 min. These capacities are comparable to those measured isothermally (1.40 mmol/g and 0.72 mmol/g, respectively, Figure 3a). The slower adsorption kinetics observed for DAC compared to higher % CO_2 streams can be attributed in part to the longer time needed for sufficient CO_2 to flow through and saturate the adsorbent (SI Table S6). Compared to the commercial amine-based polymer Lewatit R VP OC 1065, Rb_2CO_3 CD-MOF ST exhibits a similar adsorption capacity after 200 min (0.76 mmol/g for Rb_2CO_3 CD-MOF ST vs. 0.70 mmol/g for Lewatit R VP OC 1065) and faster adsorption kinetics (SI Figure S48). Rb_2CO_3 CD-MOF ST also exhibits a comparable CO_2 capacity to other OH^--based materials that have been previously studied for DAC (SI Table S8).

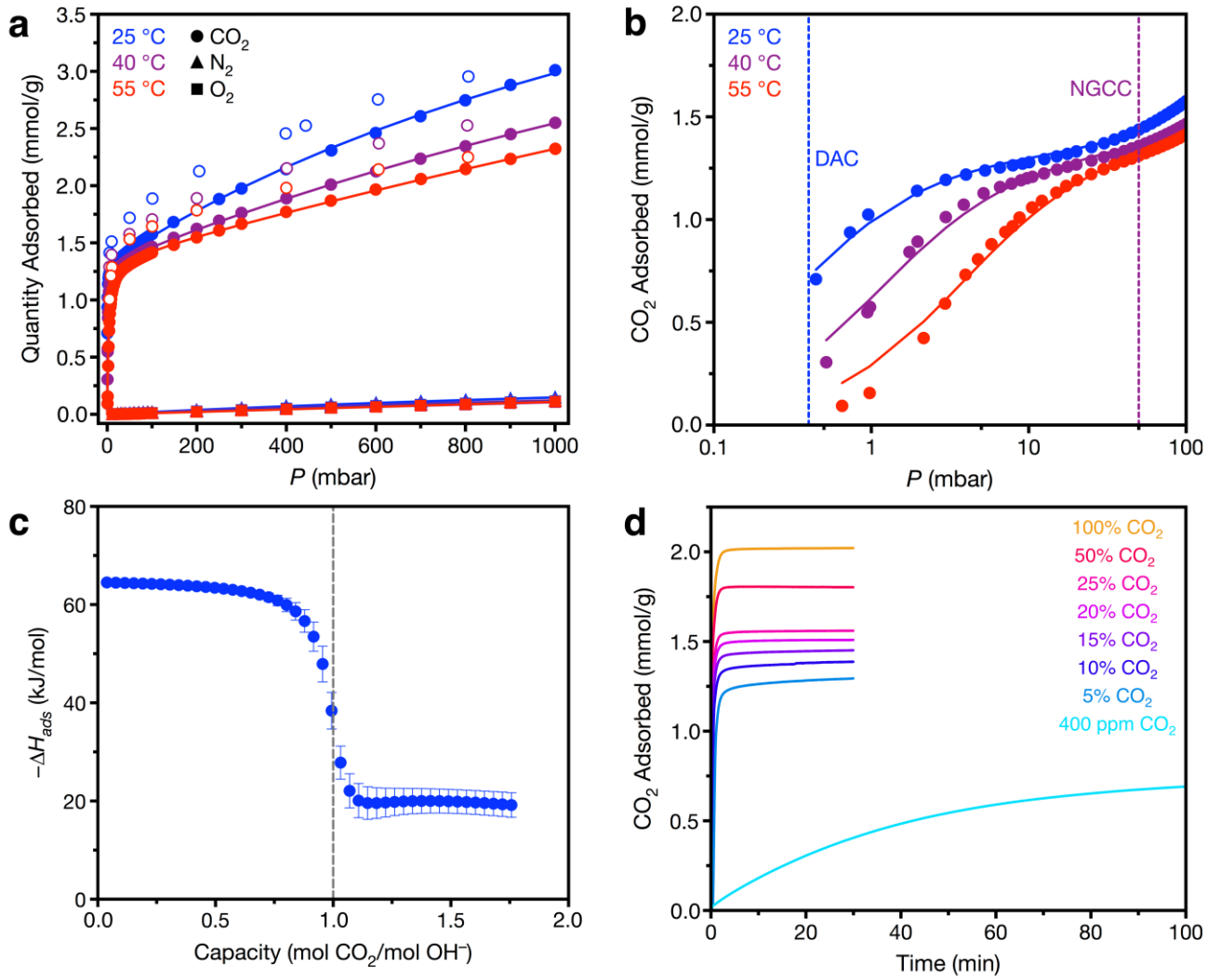

Figure 3. a) CO_2 (circles), N_2 (triangles), and O_2 (squares) adsorption (closed) and desorption (open) isotherms of Rb_2CO_3 CD-MOF ST at 25 °C (blue), 40 °C (purple), and 55 °C (red). Solid lines represent fits to the dual-site Langmuir-Freundlich model. Samples were reactivated at 25 °C for 24 h under high vacuum (<10 μbar) between isotherms. A data point was considered equilibrated when less than 0.01% change in pressure occurred over a 45 s interval. b) CO_2 adsorption isotherms of Rb_2CO_3 CD-MOF ST in the low-pressure regime. Dashed lines corresponding to the partial pressures of CO_2 in air (0.4 mbar CO_2, 25 °C) and NGCC flue gas (50 mbar, 40 °C) are indicated. c) $-\Delta H_{ads}$ for Rb_2CO_3 CD-MOF ST determined using the Clausius-Clapeyron equation and the fits in Figure 3a. The dashed line corresponds to a capacity of 1 CO_2 per OH^- site. d) CO_2 adsorption profiles of Rb_2CO_3 CD-MOF ST from various mixtures of CO_2 in N_2 (5–100%) or CO_2 in air (400 ppm), as measured by TGA at a flow rate of 60 mL/min. N_2 adsorption is assumed to be negligible.

The promising performance of Rb_2CO_3 CD-MOF ST for carbon capture from air and NGCC emissions encouraged us to evaluate its cycling performance in a simulated temperature-pressure swing process using a N_2 purge as a stand-in for a pressure swing due to instrument limitations (Figure 4).[60] As such, Rb_2CO_3 CD-MOF ST was subjected to 10 adsorption (dry 400 ppm CO_2 in air, 25 °C) and desorption (dry N_2, 80 °C) cycles via TGA (Figure 4a, see Figure S22 for the full cycling data). The cycled CO_2 working capacity (~0.7 mmol/g) is comparable to that measured in the adsorption isotherm (0.72 mmol/g, Figure 3b). Consistent with the accelerated decomposition test results (Figure 2b), Rb_2CO_3 CD-MOF ST is stable upon cycling, retaining 97% of its capacity after 10 DAC cycles. Next, Rb_2CO_3 CD-MOF ST was subjected to 100 adsorption (dry 5% CO_2 in N_2, 40 °C) and desorption (dry N_2, 80 °C) cycles in a simulated carbon capture process from a NGCC emission stream (Figure 4b). The CO_2 working capacity (~1.3 mmol/g) is again similar to that measured under ideal conditions in the adsorption isotherm (1.40 mmol/g, Figure 3b). Rb_2CO_3 CD-MOF ST retains >90% of its capacity after 100 cycles, further reflecting its excellent thermal stability. When investigating the cause of the slight decrease in the capacity of Rb_2CO_3 CD-MOF ST upon cycling, we noticed that it was not losing mass (as might be expected if the material was degrading) but instead was showing signs of partially irreversible CO_2 uptake. This can be best visualized using linear fits to the adsorption (blue), desorption (red), and cycling (black) capacities in Figure 4b. The slope corresponding to the decrease in cycling capacity (–0.0013 mmol/g•cycle) matches well to the slope corresponding to the gradual increase in the desorption capacity upon cycling (+0.0010 mmol/g•cycle). This finding suggests that desorption of CO_2 from this material is slightly irreversible upon cycling under dry conditions (see further discussion below).

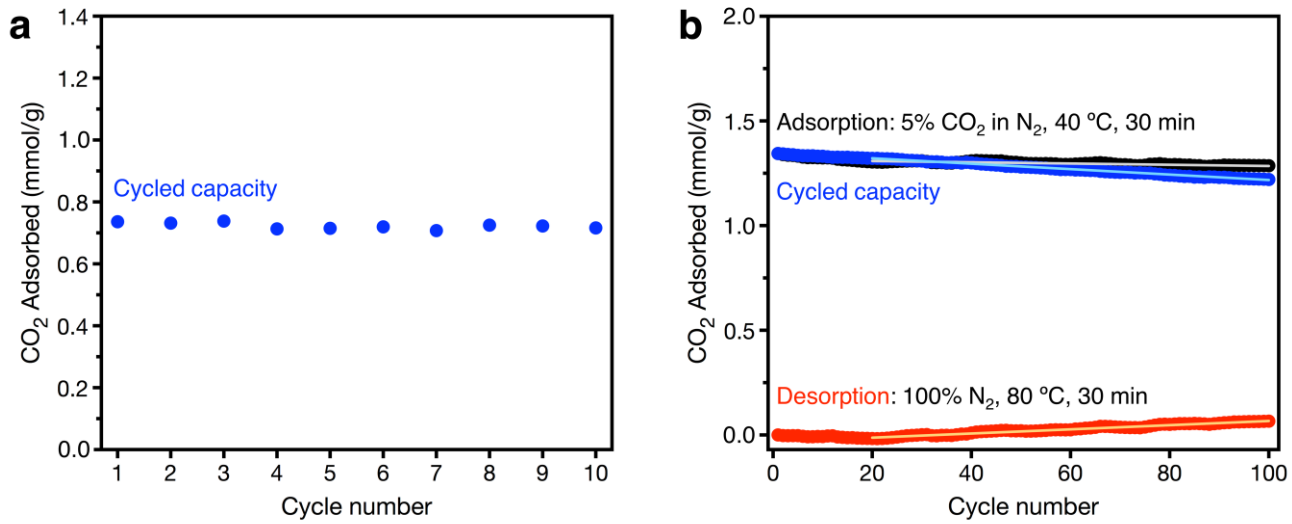

Figure 4. a) Cycling capacities for 10 adsorption/desorption cycles for Rb_2CO_3 CD-MOF ST in a simulated temperature-pressure swing DAC process. Adsorption: dry 400 ppm CO_2 in air, 25 °C, 200 min. Desorption: dry, pure N_2, 80 °C, 30 min; dry air, 25 °C, 30 min. The cycled capacity (difference) is shown. See SI Figure S36 for full cycling data. b) Cycling data for 100 adsorption/desorption cycles for Rb_2CO_3 CD-MOF in a simulated temperature-pressure swing NGCC CCUS process. The slopes of the linear trendlines for the cycled capacity data (blue), adsorption data (black), and desorption data (red) are –0.0013, –0.0003, and +0.0010 mmol/g•cycle, respectively. N_2 adsorption is assumed to be negligible.

To evaluate the performance of Rb_2CO_3 CD-MOF ST in a more realistic fixed-bed adsorption process, multi-component breakthrough experiments were conducted with dry simulated NGCC flue gas (5% CO_2 in N_2) using a custom-built apparatus (Figure 5, see SI Section 6 for details). Breakthrough experiments were carried out by subjecting 0.387 g of activated Rb_2CO_3 CD-MOF ST to 3 sccm of dry 5% CO_2 in N_2 at 40 °C (Figure 5a). Under these conditions, N_2 broke through the column nearly instantly, followed much later by CO_2. Importantly, the CO_2 breakthrough profile was sharp, reflecting the favorable adsorption kinetics in this material (Figure 3d). The breakthrough CO_2 capacity was calculated to be 1.22 mmol/g (average of three experiments), which is comparable to the uptake under isobaric (1.30 mmol/g, Figure 3d) and isothermal (1.40 mmol/g, Figure 3b) conditions. Consistent with the 40 °C N_2 adsorption isotherm of this material (Figure 3a), its N_2 capacity was found to be negligible (<0.1 mmol/g). The breakthrough profile and capacity of Rb_2CO_3 CD-MOF ST were reproducible over three cycles following re-activation of the material at 40 °C under flowing dry He. Taken together, these gas sorption, cycling, and breakthrough measurements support that Rb_2CO_3 CD-MOF ST is a promising material for carbon capture from dilute streams under dry conditions.

All the measurements presented thus far were carried out in the absence of H_2O, yet air and NGCC flue gas generally contain significant amounts of H_2O. As such, the ability of Rb_2CO_3 CD-MOF ST to capture CO_2 from a humidified 5% CO_2 in N_2

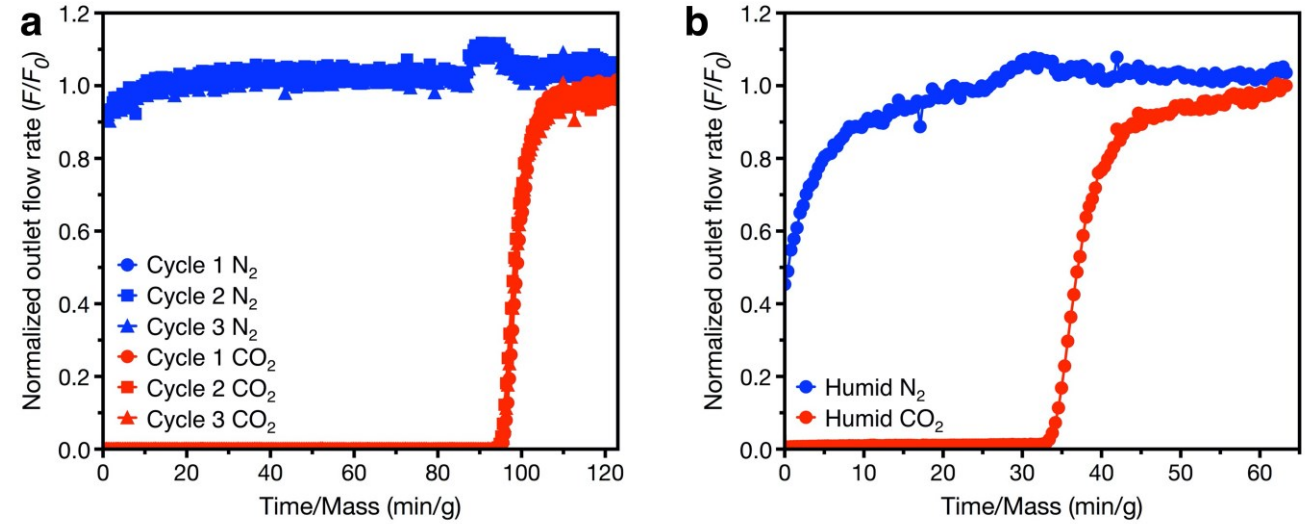

Figure 5. a) Dry breakthrough experiments with 0.387 g Rb_2CO_3 CD-MOF ST under 3 sccm of dry 5% CO_2 in N_2 at 40 °C. CO_2 capacities: 1.22, 1.22, and 1.21 mmol/g for cycles 1, 2, and 3, respectively. N_2 capacities: <0.1 mmol/g in all cases. b) Humid breakthrough measurement (46% relative humidity at 20 °C) under the same conditions. CO_2 capacity: 0.416 mmol/g. N_2 capacity: <0.1 mmol/g. The MOF was pre-humidified by flowing humid He through it until H_2O was detected by RGA. All breakthrough measurements are corrected using the system dead time estimated by measuring the breakthrough time of Ar.

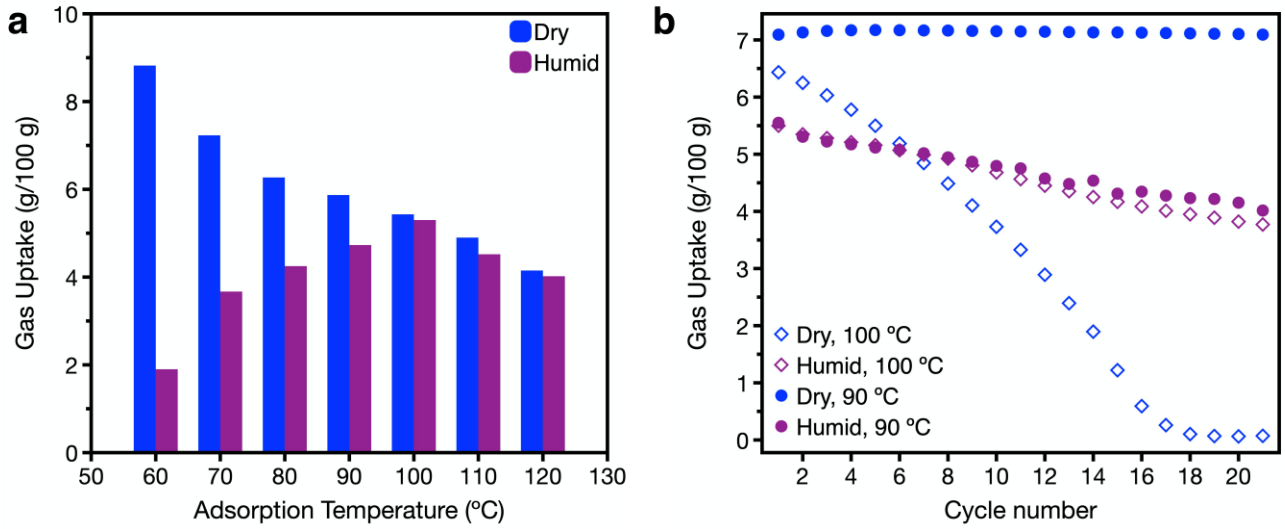

Figure 6. a) Dry (blue) and humid (15% relative humidity at 20 °C, purple) pure CO_2 uptake capacities measured by TGA after 30 min at a flow rate of 60 mL/min. b) Cycling capacities for 21 adsorption/desorption cycles for Rb_2CO_3 CD-MOF ST in a simulated isothermal, high-temperature carbon capture process under dry (blue) or humid (purple) conditions. Adsorption: pure CO_2, 90 °C or 100 °C, 5 min. Desorption: pure N_2, 90 °C or 100 °C, 55 min. The cycled capacity (difference) is shown. See SI Figure S38-S39 for full cycling data.

stream (~46% relative humidity at 20 °C) was evaluated using breakthrough measurements (Figure 5b). First, the MOF was pre-saturated with H_2O by flowing humidified He through it until H_2O was detected in the effluent stream using a residual gas analyzer (RGA). After saturation, the inlet stream was switched to a humidified 5% CO_2 in N_2 stream, and the breakthrough measurement was carried out. Promisingly, Rb_2CO_3 CD-MOF ST still showed excellent CO_2/N_2 selectivity and a sharp breakthrough profile under these conditions, albeit with an attenuated CO_2 capacity (0.416 mmol/g) compared to that obtained under dry conditions (1.22 mmol/g). The delayed breakthrough time of N_2 in the humid measurement can be attributed to the humidified N_2 taking longer to reach the RGA due to pore-clogging from the water in the MOF, as opposed to increased N_2 adsorption. H_2O adsorption measurements at 25 °C suggest this is likely due to strong water uptake leading to pore clogging at low temperatures (SI Figures S26–S27).

Given the strong CO_2 affinity of Rb_2CO_3 CD-MOF ST, we hypothesized that it might show improved CO_2 capture from humidified streams at elevated temperatures, where H_2O physisorption should be suppressed.[55] To evaluate this possibility, dry and humid (~15% relative humidity at 20 °C) pure CO_2 uptake profiles were collected via TGA at temperatures ranging from 40 °C to 140 °C (Figures 6a and 7a, SI Figure S41, Table S7). Under dry conditions, the expected behavior for a Langmuir adsorbent—decreasing adsorption capacity at higher adsorption temperatures—was observed (Figure 6a, blue). Nonetheless, the pure CO_2 adsorption capacity of Rb_2CO_3 CD-MOF ST at 120 °C is still quite high (0.91 mmol/g or 4.0 g/100 g,), reflecting its strong interaction with CO_2. The material also saturates with CO_2 within 2 min at every tested temperature (Figure 7a).

Although TGA cannot necessarily discriminate between the (co-)adsorption of CO_2 and H_2O, in the humid TGA measurements, Rb_2CO_3 CD-MOF ST was pre-saturated with H_2O under flowing humid N_2 at the indicated temperature before switching the gas stream to humid CO_2, allowing us to attribute the majority of the observed mass increase to CO_2 adsorption (purple, Figure 6b). Consistent with the humid breakthrough results (Figure 5b), attenuated uptake (1.57 g/100 g, 0.397 mmol/g if all CO_2) was observed at 40 °C under humid conditions compared to dry conditions (8.67 g/100 g) (SI Figure S41). The observed capacity at 40 °C via humid TGA is similar to that measured via breakthrough from a humid 5% CO_2 in N_2 stream (0.412 mmol/g, Figure 5b), supporting that the observed uptake in the humid TGA measurement is largely due to CO_2 adsorption. Even so, we cannot rule out that some co-adsorption of H_2O occurs under the tested conditions. In contrast to the dry CO_2 uptake results, increasing the temperature up to 100 °C under humid conditions led to greater CO_2 uptake. This is likely due to reduced H_2O adsorption at higher temperatures, allowing for more efficient CO_2 capture. Between 100–120 °C, the dry and humid CO_2 uptake capacities are nearly identical, supporting that Rb_2CO_3 CD-MOF ST is capable of selectively removing CO_2 from humid streams at elevated temperatures. Notably, rapid CO_2 adsorption was still observed in humidified Rb_2CO_3 CD-MOF ST, with saturation reached in 5 min at all tested temperatures (SI Figure S41). Overall, these findings suggest that OH^--based adsorbents like Rb_2CO_3 CD-MOF ST may be best suited for carbon capture from humid streams in an intermediate temperature regime (80–120 °C), given that many of them struggle to capture CO_2 efficiently from humid streams at lower temperatures.[42,47]

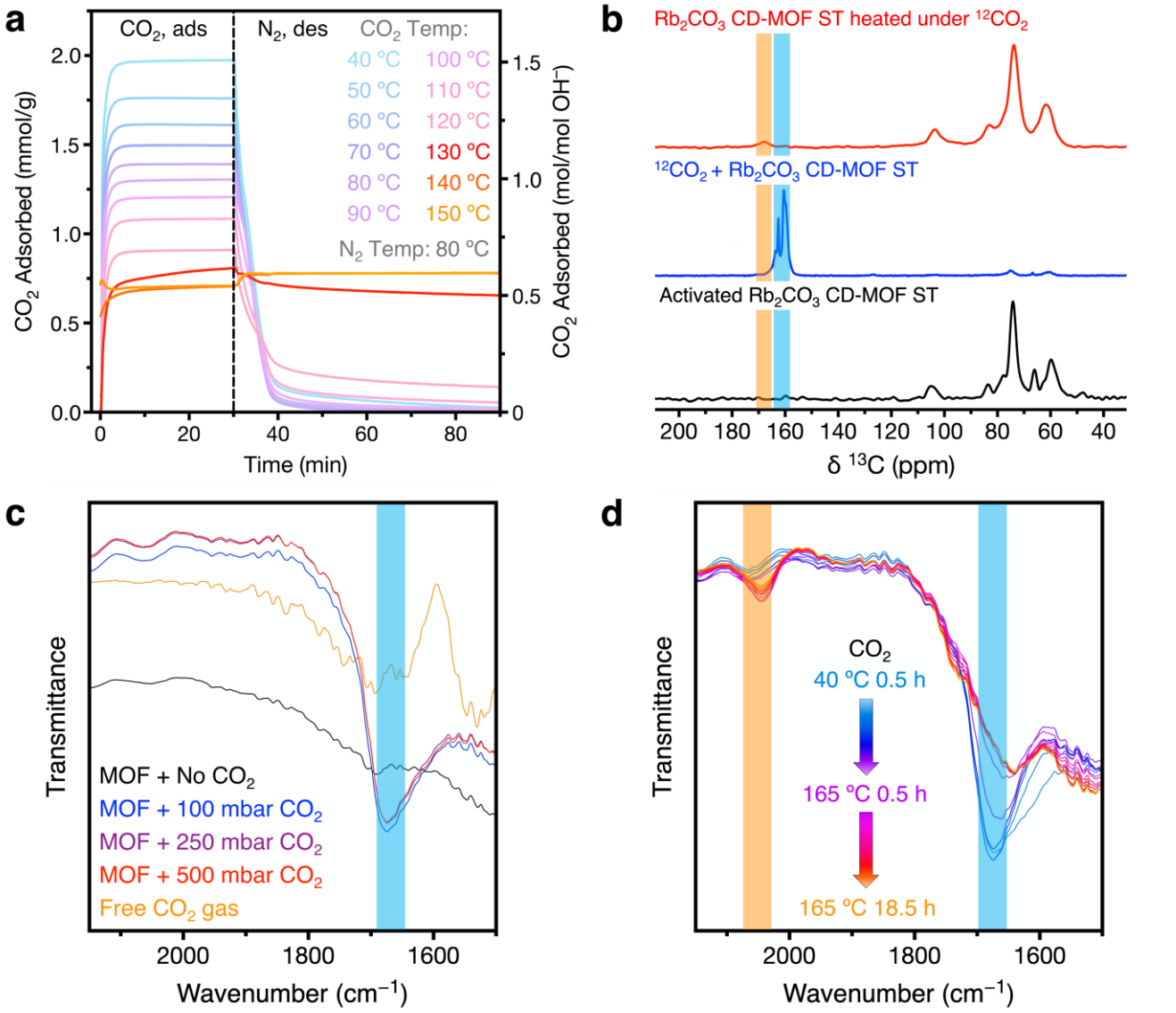

Figure 7. Irreversible CO_2 uptake experiments. a) Dry, pure CO_2 adsorption profiles of Rb_2CO_3 CD-MOF ST at various temperatures (40−150 °C, left) and associated dry N_2 desorption profiles at 80 °C (right), as measured by TGA. b) ^{13}C proton-decoupled Hahn echo NMR spectra of activated Rb_2CO_3 CD-MOF ST (black), Rb_2CO_3 CD-MOF ST after dosing with $^{13}CO_2$ at room temperature (blue), and after heating under dry $^{12}CO_2$ flow for 2 h (red). All SSNMR measurements were conducted at a field strength of 9.4 T and a spinning rate of 20 kHz. The resonances corresponding to HCO_3^- (blue) and CO_3^{2-} (orange) are indicated. DRIFTS profiles of Rb_2CO_3 CD-MOF ST under CO_2 c) at room temperature and d) upon heating to 165 °C and standing at this temperature for 18.5 h. The stretches corresponding to HCO_3^- (blue) and CO_3^{2-} (orange) species are indicated.

Isothermal cycling experiments were conducted at 90 °C and 100 °C to further compare the high-temperature CO_2 capture performance of Rb_2CO_3 CD-MOF ST under both dry and humid conditions (Figure 6b, see SI Figure S39 for full cycling data). The MOF was subjected to 21 adsorption (100% CO_2, 90 °C or 100 °C, 5 min) and desorption (N_2, 90 °C or 100 °C, 55 min) cycles via TGA. Longer desorption times than those employed at lower temperatures (30 min, Figure 4) were needed to fully desorb H_2O under humid conditions, but shorter adsorption times (5 min) could be employed (to maintain an overall 1 h cycle time) due to the fast adsorption kinetics of this material at all temperatures. Under humid conditions, Rb_2CO_3 CD-MOF ST retained >70% of its original working capacity after 20 cycles at both 90 °C and 100 °C, reflecting good performance for CO_2 capture from hot, humid streams. Unexpectedly, the results obtained under dry conditions were drastically different at the two temperatures: at 90 °C, excellent cycling stability was observed, but at 100 °C, the CO_2 uptake declined significantly, reaching near 0% retention of the original capacity after 18 cycles (Figure 6b). Notably, Rb_2CO_3 CD-MOF ST retains crystallinity upon heating under pure CO_2 at 140 °C for 2 h, indicating that this irreversible uptake is not due to framework degradation (SI Figure S46). This finding suggests that, at ≥100 °C, Rb_2CO_3 CD-MOF ST shows improved cycling stability under humid conditions than under dry conditions. To the best of our knowledge, this phenomenon has not been reported to date in any OH^--based adsorbent.

The mechanistic underpinnings of the irreversible CO_2 uptake upon cycling Rb_2CO_3 CD-MOF ST under dry hot CO_2 at ≥100 °C were interrogated using gas-sorption and spectroscopic

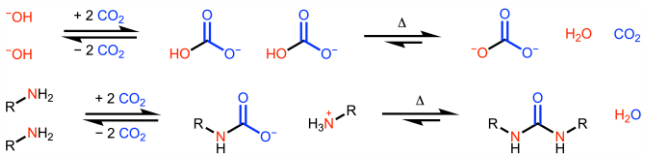

Figure 8. Proposed mechanistic switch from HCO_3^- at low temperatures to CO_3^{2-} at high temperatures under CO_2 flow in Rb_2CO_3 CD-MOF ST (top), compared to urea formation in amine-functionalized solids under similar conditions (bottom).

methods (Figure 7). Heating Rb_2CO_3 CD-MOF ST to ≥130 °C under both dry (Figure 7a) and humid (SI Figure S40) flowing CO_2 leads to irreversible CO_2 uptake. This trend can be best visualized using the CO_2 adsorption/desorption profiles; switching the inlet gas from dry, pure CO_2 at 130, 140, or 150 °C to pure N_2 at 80 °C did not result in full desorption of CO_2 and return to the initial sample mass (Figure 7a). This finding is consistent with the slightly irreversible CO_2 uptake observed upon cycling with 40 °C CO_2 under dry conditions (Figure 4b). Similarly, a significant loss in capacity due to irreversible uptake was observed when Rb_2CO_3 CD-MOF ST was subjected to 10 adsorption (dry 5% CO_2 in N_2, 40 °C) and desorption (dry 100% CO_2, 145 °C) cycles in a simulated temperature-swing adsorption process (SI Figure S37).

We hypothesized that extended exposure to hot, dry CO_2 could be mediating conversion of two adjacent HCO_3^- sites to one CO_3^{2-} species with concomitant loss of water and CO_2, akin to what happens when $KHCO_3$ is heated to produce K_2CO_3 and H_2O (Figure 8, top).[61] The reverse reaction is proposed to govern CO_2 capture in moisture-swing sorbents,[62–65] but a clear mechanistic switch from HCO_3^- to CO_3^{2-} upon cycling a OH^--based sorbent has not been reported to date. Nonetheless, similar phenomena have been observed upon cycling amine-functionalized silicas under dry conditions due to a change in mechanism from reversible ammonium carbamate to irreversible urea formation (Figure 8, bottom).[56] This hypothesis would also explain why Rb_2CO_3 CD-MOF ST shows improved cycling stability at high temperatures in the presence of H_2O (Figure 6b), which should suppress H_2O loss from HCO_3^- to form CO_3^{2-}.

Consistent with this hypothesis, the irreversible mass gain of Rb_2CO_3 CD-MOF ST at 140–150 °C stabilizes at a capacity of approximately 0.5 mol CO_2 per mol OH^-, as would be expected if two adjacent OH^- sites were reacting with CO_2 to produce one CO_3^{2-} species (Figure 7a). Similarly, the irreversible uptake of this material in a simulated temperature-swing adsorption process (with desorption under dry, pure CO_2 at 145 °C) also stabilizes at a capacity corresponding to 1 CO_2 per 2 OH^- sites (SI Figure S37). Irreversible CO_3^{2-} formation in Rb_2CO_3 CD-MOF ST at high temperatures is further supported by TGA decomposition measurements (SI Figure S28). When heated under dry flowing N_2, Rb_2CO_3 CD-MOF ST shows no significant weight change until approximately 225 °C, when it undergoes decomposition. Markedly different behavior was observed upon heating Rb_2CO_3 CD-MOF ST under dry, pure CO_2. Between 135 °C and 200 °C, the mass of this sample stabilizes at a value corresponding to 1 CO_2 per 2 OH^- sites. Together, these thermogravimetric measurements support that CO_2 capture in Rb_2CO_3 CD-MOF ST occurs via reversible HCO_3^- formation at low temperatures, but at high temperatures and upon cycling under dry conditions, a switch in mechanism occurs to irreversibly form CO_3^{2-} species with concomitant loss of H_2O.

To test the hypothesis of CO_3^{2-} formation in Rb_2CO_3 CD-MOF ST at high temperatures under CO_2 flow, we performed magic angle spinning (MAS) ^{13}C SSNMR (Figure 7b, see SI Section 8 for details) and DRIFTS measurements (Figure 7c–d, see SI Section 5 for details). The proton-decoupled Hahn echo MAS ^{13}C SSNMR spectrum of activated Rb_2CO_3 CD-MOF ST only contains resonances corresponding to the γ-CD units, as expected (Figure 7b, black).[66] Dosing this MOF with $^{13}CO_2$ at room temperature leads to the appearance of a complex set of resonances centered at ~160 ppm (Figure 7b, blue). This chemical shift range is generally indicative of HCO_3^-, as it is similar to the chemical shift of $KHCO_3$ (161 ppm) as well as HCO_3^- species formed in OH^--charged porous carbons (156 ppm).[67] The complexity of this signal suggests that multiple chemisorbed species form upon CO_2 dosing, which is likely due to the presence of different hydrogen-bonding environments provided by the neighboring γ-CD units. Heating Rb_2CO_3 CD-MOF ST under dry, hot $^{12}CO_2$ flow for 2 h (used instead of $^{13}CO_2$ due to cost) led to the complete disappearance of these resonances and the appearance of a single new resonance centered at 168 ppm (Figure 7c, red). This chemical shift is consistent with CO_3^{2-}, as it is identical to the chemical shift of K_2CO_3 (168 ppm).[68] Additionally, in cross-polarized (CP) MAS SSNMR experiments, the carbonate signal is not observed due to the absence of any nearby protons, further supporting its assignment as CO_3^{2-} (SI Figure S60). Thus, our CP MAS ^{13}C SSNMR spectroscopic studies support the unprecedented mechanistic switch from HCO_3^- to CO_3^{2-} upon heating Rb_2CO_3 CD-MOF ST under hot, dry CO_2.

To further verify these assignments, DRIFTS spectra of Rb_2CO_3 CD-MOF ST were collected under four conditions: (1) dry N_2 at room temperature (black, Figure 7c), (2) under increasing pressures of dry CO_2 at room temperature (Figure 7c), (3) under flowing dry, pure CO_2 at temperatures between 40 °C and 165 °C, and (4) under flowing CO_2 for 18.5 h at 165 °C (Figure 7d). The DRIFTS spectra of Rb_2CO_3 CD-MOF ST after dosing with CO_2 at room temperature contain a clear new C=O stretch at 1675 cm^{-1} that is absent in the parent MOF (highlighted in blue, Figure 7c). This stretch is consistent with the C=O stretch in pure $KHCO_3$ (1683 cm^{-1}, SI Figure S49) and thus is assigned to a HCO_3^- species.[42] Upon heating under flowing dry CO_2, this peak is preserved but with slightly decreased intensity (Figure 7d). Above 140 °C, the HCO_3^- stretch begins to decrease in intensity, and a new stretch appears at 1645 cm^{-1} (highlighted in orange), which is similar to the CO_3^{2-} stretch in pure K_2CO_3 (1649 cm^{-1}) and Rb_2CO_3 (1650 cm^{-1}) (SI Figure S49). Heating the material under flowing CO_2 at 165 °C causes the HCO_3^- stretch at 1675 cm^{-1} to gradually disappear and the CO_3^{2-} stretch at 1645 cm^{-1} to further increase in intensity, along with the growth of a new stretch at 2045 cm^{-1} (orange box). The stretch at 2045 cm^{-1} is present in the DRIFTS spectra of K_2CO_3 and Rb_2CO_3 but not $KHCO_3$ (SI Figure S49) and is likely a combination band, which are diagnostic of carbonate minerals.[69,70] As such, these DRIFTS spectra further support a gradual transition from HCO_3^- to CO_3^{2-} upon prolonged heating of Rb_2CO_3 CD-MOF ST under dry CO_2.

Taken together, these gas sorption and spectroscopic studies strongly support a temperature-based change in adsorption mechanism in Rb_2CO_3 CD-MOF ST, from reversible formation of HCO_3^- at low temperatures to irreversibly formed CO_3^{2-} at high temperatures and/or upon prolonged cycling. This parasitic mechanism has important implications for the performance of OH^--based sorbents under both dry and humid conditions, as it

seems that the presence of H_2O can somewhat suppress CO_3^{2-} formation at high temperatures (Figure 6b). The same phenomenon has also been observed for amine-functionalized silicas that are prone to urea formation under dry conditions.[56]

Conclusion.

The OH^--based framework Rb_2CO_3 CD-MOF ST possesses high CO_2 capacities from dilute streams such as air and NGCC emissions while exhibiting excellent oxidative, thermal, and cycling stabilities and selective CO_2 capture under mixed gas conditions. Intriguingly, under humid, hot conditions, Rb_2CO_3 CD-MOF ST displays reversible CO_2 chemisorption, which is rare for OH^--based materials. However, under dry, hot conditions, the reversibly formed HCO_3^- transforms into CO_3^{2-}, which has not been previously observed in a OH^--based material. These findings suggest that Rb_2CO_3 CD-MOF ST is a promising CO_2 sorbent for DAC and high temperature NGCC emissions capture processes. In developing CO_2 capture materials, we propose that reactive OH^- sites should be spaced far apart to productively capture CO_2 without compromising reversibility upon extended cycling. Our discoveries reveal structural trends in MOFs that will aid in the design of next-generation materials containing oxygen-based nucleophiles for carbon capture from dry and humid streams.

ASSOCIATED CONTENT

Supporting Information. Details of synthetic procedures and gas sorption measurements. This material is available free of charge via the Internet at http://pubs.acs.org.

AUTHOR INFORMATION

Corresponding Author

* pjm347@cornell.edu

Present Address

[†]Davidson School of Chemical Engineering, Purdue University, West Lafayette, IN 47907, United States

[§] Department of Chemistry, Northwestern University, Evanston, IL, 60208, United States

[¶]Department of Chemistry, Hamilton College, Clinton, NY, 13323, United States

Author Contributions

[‡]These authors contributed equally.

Funding Sources

This work was supported by the U.S. Department of Energy, Office of Science, Office of Basic Energy Sciences under Award Number DE-SC0021000 (S.A.L., M.E.Z., T.A.P., R.T.J., P.J.M.). We also acknowledge support from a Camille Dreyfus Teacher-Scholar Award to P.J.M. (TC-23-048). This work made use of the Cornell Center for Materials Research Shared Facilities, which are supported through the NSF MRSEC program (DMR-1719875). ACF and BJR would like to acknowledge the support of the Leverhulme Trust Research Project Grant (RPG-2020-337). BJR also acknowledges Jesus College, Cambridge. ACF further acknowledges a UKRI Future Leaders Fellowship (MR/T043024/1).

REFERENCES

(1) Climate Change 2021: The Physical Science Basis. Contribution of Working Group I to the Sixth Assessment Report of the Intergovernmental Panel on Climate Change; Masson-Delmotte, V., Zhai, P., Pirani, A., Connors, S. L., Péan, C., Chen, Y., Goldfarb, L., Gomis, M. I., Matthews, J. B. R., Berger, S., Huang, M., Yelekçi, O., Yu, R., Zhou, B., Lonnoy, E., Maycock, T. K., Waterfield, T., Leitzell, K., Caud, Nada, Eds.; Cambridge University Press, 2021.

(2) National Oceanic & Atmospheric Administration. Trends in Atmospheric Carbon Dioxide. NOAA Global Monitoring Laboratory. https://gml.noaa.gov/ccgg/trends/gl_gr.html.

(3) Chu, S. Carbon Capture and Sequestration. *Science* **2009**, *325* (5948), 1599–1599. https://doi.org/10.1126/science.1181637.

(4) Bui, M.; Adjiman, C. S.; Bardow, A.; Anthony, E. J.; Boston, A.; Brown, S.; Fennell, P. S.; Fuss, S.; Galindo, A.; Hackett, L. A.; Hallett, J. P.; Herzog, H. J.; Jackson, G.; Kemper, J.; Krevor, S.; Maitland, G. C.; Matuszewski, M.; Metcalfe, I. S.; Petit, C.; Puxty, G.; Reimer, J.; Reiner, D. M.; Rubin, E. S.; Scott, S. A.; Shah, N.; Smit, B.; Trusler, J. P. M.; Webley, P.; Wilcox, J.; Mac Dowell, N. Carbon Capture and Storage (CCS): The Way Forward. *Energy Environ. Sci.* **2018**, *11* (5), 1062–1176. https://doi.org/10.1039/C7EE02342A.

(5) Siegelman, R. L.; Milner, P. J.; Kim, E. J.; Weston, S. C.; Long, J. R. Challenges and Opportunities for Adsorption-Based CO_2 Capture from Natural Gas Combined Cycle Emissions. *Energy Environ. Sci.* **2019**, *12* (7), 2161–2173. https://doi.org/10.1039/C9EE00505F.

(6) Zhu, X.; Xie, W.; Wu, J.; Miao, Y.; Xiang, C.; Chen, C.; Ge, B.; Gan, Z.; Yang, F.; Zhang, M.; O'Hare, D.; Li, J.; Ge, T.; Wang, R. Recent Advances in Direct Air Capture by Adsorption. *Chem. Soc. Rev.* **2022**, *51* (15), 6574–6651. https://doi.org/10.1039/D1CS00970B.

(7) McQueen, N.; Gomes, K. V.; McCormick, C.; Blumanthal, K.; Pisciotta, M.; Wilcox, J. A Review of Direct Air Capture (DAC): Scaling up Commercial Technologies and Innovating for the Future. *Prog. Energy* **2021**, *3* (3), 032001. https://doi.org/10.1088/2516-1083/abf1ce.

(8) Shi, X.; Xiao, H.; Azarabadi, H.; Song, J.; Wu, X.; Chen, X.; Lackner, K. S. Sorbents for the Direct Capture of CO_2 from Ambient Air. *Angew. Chem. Int. Ed.* **2020**, *59* (18), 6984–7006. https://doi.org/10.1002/anie.201906756.

(9) Sanz-Pérez, E. S.; Murdock, C. R.; Didas, S. A.; Jones, C. W. Direct Capture of CO_2 from Ambient Air. *Chem. Rev.* **2016**, *116* (19), 11840–11876. https://doi.org/10.1021/acs.chemrev.6b00173.

(10) Cost and Performance Baseline for Fossil Energy Plants Volume 1a: Bituminous Coal (PC) and Natural Gas to Electricity (Rev. 3); DOE/NETL-2015/1723; National Energy Technology Laboratory, 2015. https://doi.org/10.2172/1480987.

(11) The Atmosphere | National Oceanic and Atmospheric Administration. https://www.noaa.gov/jetstream/atmosphere (accessed 2024-09-07).

(12) Siegelman, R. L.; Kim, E. J.; Long, J. R. Porous Materials for Carbon Dioxide Separations. *Nature Mater.* **2021**, *20* (8), 1060–1072. https://doi.org/10.1038/s41563-021-01054-8.

(13) Amann, J.-M. G.; Bouallou, C. CO_2 Capture from Power Stations Running with Natural Gas (NGCC) and Pulverized Coal (PC): Assessment of a New Chemical Solvent Based on Aqueous Solutions of N-Methyldiethanolamine +

Triethylene Tetramine. *Energy Procedia* **2009**, *1* (1), 909–916. https://doi.org/10.1016/j.egypro.2009.01.121.
(14) Duan, Y.; Sorescu, D. C. CO_2 Capture Properties of Alkaline Earth Metal Oxides and Hydroxides: A Combined Density Functional Theory and Lattice Phonon Dynamics Study. *J. Chem. Phys.* **2010**, *133* (7), 074508. https://doi.org/10.1063/1.3473043.
(15) Mahmoudkhani, M.; Keith, D. W. Low-Energy Sodium Hydroxide Recovery for CO_2 Capture from Atmospheric Air—Thermodynamic Analysis. *Int. J. Greenhouse Gas Control* **2009**, *3* (4), 376–384. https://doi.org/10.1016/j.ijggc.2009.02.003.
(16) Carneiro, J. S. A.; Innocenti, G.; Moon, H. J.; Guta, Y.; Proaño, L.; Sievers, C.; Sakwa-Novak, M. A.; Ping, E. W.; Jones, C. W. Insights into the Oxidative Degradation Mechanism of Solid Amine Sorbents for CO_2 Capture from Air: Roles of Atmospheric Water. *Angew. Chem. Int. Ed.* **2023**, *62* (24), e202302887. https://doi.org/10.1002/anie.202302887.
(17) Jahandar Lashaki, M.; Khiavi, S.; Sayari, A. Stability of Amine-Functionalized CO_2 Adsorbents: A Multifaceted Puzzle. *Chem. Soc. Rev.* **2019**, *48* (12), 3320–3405. https://doi.org/10.1039/C8CS00877A.
(18) Buijs, W. Direct Air Capture of CO_2 with an Amine Resin: A Molecular Modeling Study of the Oxidative Deactivation Mechanism with O_2. *Ind. Eng. Chem. Res.* **2019**, *58* (38), 17760–17767. https://doi.org/10.1021/acs.iecr.9b03823.
(19) Yu, Q.; Delgado, J. D. L. P.; Veneman, R.; Brilman, D. W. F. Stability of a Benzyl Amine Based CO_2 Capture Adsorbent in View of Regeneration Strategies. *Ind. Eng. Chem. Res.* **2017**, *56* (12), 3259–3269. https://doi.org/10.1021/acs.iecr.6b04645.
(20) Didas, S. A.; Zhu, R.; Brunelli, N. A.; Sholl, D. S.; Jones, C. W. Thermal, Oxidative and CO_2 Induced Degradation of Primary Amines Used for CO_2 Capture: Effect of Alkyl Linker on Stability. *J. Phys. Chem. C* **2014**, *118* (23), 12302–12311. https://doi.org/10.1021/jp5025137.
(21) Ahmadalinezhad, A.; Sayari, A. Oxidative Degradation of Silica-Supported Polyethylenimine for CO_2 Adsorption: Insights into the Nature of Deactivated Species. *Phys. Chem. Chem. Phys.* **2014**, *16* (4), 1529–1535. https://doi.org/10.1039/C3CP53928H.
(22) Ahmadalinezhad, A.; Tailor, R.; Sayari, A. Molecular-Level Insights into the Oxidative Degradation of Grafted Amines. *Chem. Eur. J.* **2013**, *19* (32), 10543–10550. https://doi.org/10.1002/chem.201300864.
(23) Bali, S.; Chen, T. T.; Chaikittisilp, W.; Jones, C. W. Oxidative Stability of Amino Polymer–Alumina Hybrid Adsorbents for Carbon Dioxide Capture. *Energy Fuels* **2013**, *27* (3), 1547–1554. https://doi.org/10.1021/ef4001067.
(24) Fredriksen, S. B.; Jens, K.-J. Oxidative Degradation of Aqueous Amine Solutions of MEA, AMP, MDEA, Pz: A Review. *Energy Procedia* **2013**, *37*, 1770–1777. https://doi.org/10.1016/j.egypro.2013.06.053.
(25) Hallenbeck, A. P.; Kitchin, J. R. Effects of O_2 and SO_2 on the Capture Capacity of a Primary-Amine Based Polymeric CO_2 Sorbent. *Ind. Eng. Chem. Res.* **2013**, *52* (31), 10788–10794. https://doi.org/10.1021/ie400582a.
(26) Gouedard, C.; Picq, D.; Launay, F.; Carrette, P.-L. Amine Degradation in CO_2 Capture. I. A Review. *Int. J. Greenhouse Gas Control* **2012**, *10*, 244–270. https://doi.org/10.1016/j.ijggc.2012.06.015.
(27) Bollini, P.; Choi, S.; Drese, J. H.; Jones, C. W. Oxidative Degradation of Aminosilica Adsorbents Relevant to Postcombustion CO_2 Capture. *Energy Fuels* **2011**, *25* (5), 2416–2425. https://doi.org/10.1021/ef200140z.
(28) Drage, T. C.; Snape, C. E.; Stevens, L. A.; Wood, J.; Wang, J.; Cooper, A. I.; Dawson, R.; Guo, X.; Satterley, C.; Irons, R. Materials Challenges for the Development of Solid Sorbents for Post-Combustion Carbon Capture. *J. Mater. Chem.* **2012**, *22* (7), 2815–2823. https://doi.org/10.1039/C2JM12592G.
(29) Rochelle, G. T. Amine Scrubbing for CO_2 Capture. *Science* **2009**, *325* (5948), 1652–1654. https://doi.org/10.1126/science.1176731.
(30) Hamdy, L. B.; Goel, C.; Rudd, J. A.; Barron, A. R.; Andreoli, E. The Application of Amine-Based Materials for Carbon Capture and Utilisation: An Overarching View. *Mater. Adv.* **2021**, *2* (18), 5843–5880. https://doi.org/10.1039/D1MA00360G.
(31) Ünveren, E. E.; Monkul, B. Ö.; Sarıoğlan, Ş.; Karademir, N.; Alper, E. Solid Amine Sorbents for CO_2 Capture by Chemical Adsorption: A Review. *Petroleum* **2017**, *3* (1), 37–50. https://doi.org/10.1016/j.petlm.2016.11.001.
(32) Veneman, R.; Zhao, W.; Li, Z.; Cai, N.; Brilman, D. W. F. Adsorption of CO_2 and H_2O on Supported Amine Sorbents. *Energy Procedia* **2014**, *63*, 2336–2345. https://doi.org/10.1016/j.egypro.2014.11.254.
(33) Bollini, P.; Didas, S. A.; Jones, C. W. Amine-Oxide Hybrid Materials for Acid Gas Separations. *J. Mat. Chem.* **2011**, *21* (39), 15100. https://doi.org/10.1039/c1jm12522b.
(34) Keith, D. W.; Holmes, G.; St. Angelo, D.; Heidel, K. A Process for Capturing CO_2 from the Atmosphere. *Joule* **2018**, *2* (8), 1573–1594. https://doi.org/10.1016/j.joule.2018.05.006.
(35) Samari, M.; Ridha, F.; Manovic, V.; Macchi, A.; Anthony, E. J. Direct Capture of Carbon Dioxide from Air via Lime-Based Sorbents. *Mitig. Adapt. Strateg. Glob. Change* **2020**, 25 (1), 25–41. https://doi.org/10.1007/s11027-019-9845-0.
(36) Erans, M.; Sanz-Pérez, E. S.; Hanak, D. P.; Clulow, Z.; Reiner, D. M.; Mutch, G. A. Direct Air Capture: Process Technology, Techno-Economic and Socio-Political Challenges. *Energy Environ. Sci.* **2022**, *15* (4), 1360–1405. https://doi.org/10.1039/D1EE03523A.
(37) McQueen, N.; Gomes, K. V.; McCormick, C.; Blumanthal, K.; Pisciotta, M.; Wilcox, J. A Review of Direct Air Capture (DAC): Scaling up Commercial Technologies and Innovating for the Future. *Prog. Energy* **2021**, *3* (3), 032001. https://doi.org/10.1088/2516-1083/abf1ce.
(38) Gambhir, A.; Tavoni, M. Direct Air Carbon Capture and Sequestration: How It Works and How It Could Contribute to Climate-Change Mitigation. *One Earth* **2019**, *1* (4), 405–409. https://doi.org/10.1016/j.oneear.2019.11.006.
(39) Peng, Y.; Zhao, B.; Li, L. Advance in Post-Combustion CO_2 Capture with Alkaline Solution: A Brief Review. *Energy Procedia* **2012**, *14*, 1515–1522. https://doi.org/10.1016/j.egypro.2011.12.1126.
(40) Wang, T.; Liu, J.; Lackner, K. S.; Shi, X.; Fang, M.; Luo, Z. Characterization of Kinetic Limitations to Atmospheric CO_2 Capture by Solid Sorbent: Characterization of Kinetic Limitations to Atmospheric CO_2 Capture by Solid Sorbent. *Greenhouse Gas Sci. Technol.* **2016**, *6* (1), 138–149. https://doi.org/10.1002/ghg.1535.
(41) Wang, T.; Liu, J.; Fang, M.; Luo, Z. A Moisture Swing Sorbent for Direct Air Capture of Carbon Dioxide: Thermodynamic and Kinetic Analysis. *Energy Procedia* **2013**, *37*, 6096–6104. https://doi.org/10.1016/j.egypro.2013.06.538.
(42) Zick, M. E.; Pugh, S. M.; Lee, J.-H.; Forse, A. C.; Milner, P. J. Carbon Dioxide Capture at Nucleophilic Hydroxide Sites in Oxidation-Resistant Cyclodextrin-Based Metal-Organic Frameworks. *Angew. Chem. Int. Ed.* **2022**, 61 (30), e202206718. https://doi.org/10.1002/anie.202206718.

(43) Lyu, H.; Chen, O. I.-F.; Hanikel, N.; Hossain, M. I.; Flaig, R. W.; Pei, X.; Amin, A.; Doherty, M. D.; Impastato, R. K.; Glover, T. G.; Moore, D. R.; Yaghi, O. M. Carbon Dioxide Capture Chemistry of Amino Acid Functionalized Metal–Organic Frameworks in Humid Flue Gas. *J. Am. Chem. Soc.* **2022**, *144* (5), 2387–2396. https://doi.org/10.1021/jacs.1c13368.

(44) Bien, C. E.; Cai, Z.; Wade, C. R. Using Postsynthetic X-Type Ligand Exchange to Enhance CO_2 Adsorption in Metal–Organic Frameworks with Kuratowski-Type Building Units. *Inorg. Chem.* **2021**, *60* (16), 11784–11794. https://doi.org/10.1021/acs.inorgchem.1c01077.

(45) Cai, Z.; Bien, C. E.; Liu, Q.; Wade, C. R. Insights into CO_2 Adsorption in M–OH Functionalized MOFs. *Chem. Mater.* **2020**, *32* (10), 4257–4264. https://doi.org/10.1021/acs.chemmater.0c00746.

(46) Bien, C. E.; Liu, Q.; Wade, C. R. Assessing the Role of Metal Identity on CO_2 Adsorption in MOFs Containing M–OH Functional Groups. *Chem. Mater.* **2020**, 32 (1), 489–497. https://doi.org/10.1021/acs.chemmater.9b04228.

(47) Bien, C. E.; Chen, K. K.; Chien, S.-C.; Reiner, B. R.; Lin, L.-C.; Wade, C. R.; Ho, W. S. W. Bioinspired Metal–Organic Framework for Trace CO_2 Capture. *J. Am. Chem. Soc.* **2018**, *140* (40), 12662–12666. https://doi.org/10.1021/jacs.8b06109.

(48) Wright, A. M.; Wu, Z.; Zhang, G.; Mancuso, J. L.; Comito, R. J.; Day, R. W.; Hendon, C. H.; Miller, J. T.; Dincă, M. A Structural Mimic of Carbonic Anhydrase in a Metal-Organic Framework. *Chem* **2018**, *4* (12), 2894–2901. https://doi.org/10.1016/j.chempr.2018.09.011.

(49) Patel, H. A.; Islamoglu, T.; Liu, Z.; Nalluri, S. K. M.; Samanta, A.; Anamimoghadam, O.; Malliakas, C. D.; Farha, O. K.; Stoddart, J. F. Noninvasive Substitution of K^+ Sites in Cyclodextrin Metal–Organic Frameworks by Li^+ Ions. *J. Am. Chem. Soc.* **2017**, *139* (32), 11020–11023. https://doi.org/10.1021/jacs.7b06287.

(50) Yan, T. K.; Nagai, A.; Michida, W.; Kusakabe, K.; Yusup, S. binti. Crystal Growth of Cyclodextrin-Based Metal-Organic Framework for Carbon Dioxide Capture and Separation. *Procedia Engineering* **2016**, *148*, 30–34. https://doi.org/10.1016/j.proeng.2016.06.480.

(51) Liao, P.-Q.; Chen, H.; Zhou, D.-D.; Liu, S.-Y.; He, C.-T.; Rui, Z.; Ji, H.; Zhang, J.-P.; Chen, X.-M. Monodentate Hydroxide as a Super Strong yet Reversible Active Site for CO_2 Capture from High-Humidity Flue Gas. Energy & Environmental *Science* **2015**, *8* (3), 1011–1016. https://doi.org/10.1039/C4EE02717E.

(52) Gassensmith, J. J.; Kim, J. Y.; Holcroft, J. M.; Farha, O. K.; Stoddart, J. F.; Hupp, J. T.; Jeong, N. C. A Metal–Organic Framework-Based Material for Electrochemical Sensing of Carbon Dioxide. *J. Am. Chem. Soc.* **2014**, *136* (23), 8277–8282. https://doi.org/10.1021/ja5006465.

(53) Wu, D.; Gassensmith, J. J.; Gouvêa, D.; Ushakov, S.; Stoddart, J. F.; Navrotsky, A. Direct Calorimetric Measurement of Enthalpy of Adsorption of Carbon Dioxide on CD-MOF-2, a Green Metal–Organic Framework. *J. Am. Chem. Soc.* **2013**, *135* (18), 6790–6793. https://doi.org/10.1021/ja402315d.

(54) Gassensmith, J. J.; Furukawa, H.; Smaldone, R. A.; Forgan, R. S.; Botros, Y. Y.; Yaghi, O. M.; Stoddart, J. F. Strong and Reversible Binding of Carbon Dioxide in a Green Metal–Organic Framework. *J. Am. Chem. Soc.* **2011**, 133 (39), 15312–15315. https://doi.org/10.1021/ja206525x.

(55) Kim, E. J.; Siegelman, R. L.; Jiang, H. Z. H.; Forse, A. C.; Lee, J.-H.; Martell, J. D.; Milner, P. J.; Falkowski, J. M.; Neaton, J. B.; Reimer, J. A.; Weston, S. C.; Long, J. R. Cooperative Carbon Capture and Steam Regeneration with Tetraamine-Appended Metal–Organic Frameworks. *Science* **2020**,*369* (6502), 392–396. https://doi.org/10.1126/science.abb397.

(56) Drage, T. C.; Arenillas, A.; Smith, K. M.; Snape, C. E. Thermal Stability of Polyethylenimine Based Carbon Dioxide Adsorbents and Its Influence on Selection of Regeneration Strategies. *Microporous Mesoporous Mater.* **2008**, *116* (1–3), 504–512. https://doi.org/10.1016/j.micromeso.2008.05.009.

(57) He, Y.; Hou, X.; Liu, Y.; Feng, N. Recent Progress in the Synthesis, Structural Diversity and Emerging Applications of Cyclodextrin-Based Metal–Organic Frameworks. *J. Mater. Chem. B* **2019**, *7* (37), 5602–5619. https://doi.org/10.1039/C9TB01548E.

(58) Smaldone, R. A.; Forgan, R. S.; Furukawa, H.; Gassensmith, J. J.; Slawin, A. M. Z.; Yaghi, O. M.; Stoddart, J. F. Metal-Organic Frameworks from Edible Natural Products. *Angew. Chem. Int. Ed.* **2010**, *49* (46), 8630–8634. https://doi.org/10.1002/anie.201002343.

(59) Liu, J.; Bao, T.-Y.; Yang, X.-Y.; Zhu, P.-P.; Wu, L.-H.; Sha, J.-Q.; Zhang, L.; Dong, L.-Z.; Cao, X.-L.; Lan, Y.-Q. Controllable Porosity Conversion of Metal-Organic Frameworks Composed of Natural Ingredients for Drug Delivery. *Chem. Commun.* **2017**, *53* (55), 7804–7807. https://doi.org/10.1039/C7CC03673F.

(60) Ebner, A. D.; Gray, M. L.; Chisholm, N. G.; Black, Q. T.; Mumford, D. D.; Nicholson, M. A.; Ritter, J. A. Suitability of a Solid Amine Sorbent for CO_2 Capture by Pressure Swing Adsorption. *Ind. Eng. Chem. Res.* **2011**, *50* (9), 5634–5641. https://doi.org/10.1021/ie2000709.

(61) Hartman, M.; Svoboda, K.; Čech, B.; Pohořelý, M.; Šyc, M. Decomposition of Potassium Hydrogen Carbonate: Thermochemistry, Kinetics, and Textural Changes in Solids. *Ind. Eng. Chem. Res.* **2019**, *58* (8), 2868–2881. https://doi.org/10.1021/acs.iecr.8b06151.

(62) Zick, M. E.; Cho, D.; Ling, J.; Milner, P. J. Carbon Capture Beyond Amines: CO_2 Sorption at Nucleophilic Oxygen Sites in Materials. *ChemNanoMat* **2023**, *9* (1), e202200436. https://doi.org/10.1002/cnma.202200436.

(63) Yang, H.; Singh, M.; Schaefer, J. Humidity-Swing Mechanism for CO_2 Capture from Ambient Air. *Chem. Commun.* **2018**, *54* (39), 4915–4918. https://doi.org/10.1039/C8CC02109K.

(64) Xiao, H.; Shi, X.; Zhang, Y.; Liao, X.; Hao, F.; Lackner, K. S.; Chen, X. The Catalytic Effect of H_2O on the Hydrolysis of CO_3^{2-} in Hydrated Clusters and Its Implication in the Humidity Driven CO_2 Air Capture. *Phys. Chem. Chem. Phys.* **2017**, *19* (40), 27435–27441. https://doi.org/10.1039/C7CP04218C.

(65) Shi, X.; Xiao, H.; Lackner, K. S.; Chen, X. Capture CO_2 from Ambient Air Using Nanoconfined Ion Hydration. *Angew. Chem. Int. Ed.* **2016**, *55* (12), 4026–4029. https://doi.org/10.1002/anie.201507846.

(66) Tseng, W.-Y.; Chen, Y.-H.; Khairullin, I. I.; Cheng, S.; Hwang, L.-P. NMR Study of Solid C_{60}(γ-Cyclodextrin)$_2$. *Solid State Nuclear Magnetic Resonance* **1997**, 8 (4), 219–229. https://doi.org/10.1016/S0926-2040(97)00013-1.

(67) Li, H.; Zick, M. E.; Trisukhon, T.; Signorile, M.; Liu, X.; Eastmond, H.; Sharma, S.; Spreng, T. L.; Taylor, J.; Gittins, J. W.; Farrow, C.; Lim, S. A.; Crocellà, V.; Milner, P. J.; Forse, A. C. Capturing Carbon Dioxide from Air with Charged-Sorbents. *Nature* **2024**, *630* (8017), 654–659. https://doi.org/10.1038/s41586-024-07449-2.

(68) Fu, R.; Cross, T. A. Solid-State Nuclear Magnetic Resonance Investigation of Protein and Polypeptide Structure. *Annual Review of Biophysics* **1999**, 28 (Volume 28, 1999),

235–268. https://doi.org/10.1146/annurev.biophys.28.1.235.
(69) Ji, J.; Ge, Y.; Balsam, W.; Damuth, J. E.; Chen, J. Rapid Identification of Dolomite Using a Fourier Transform Infrared Spectrophotometer (FTIR): A Fast Method for Identifying Heinrich Events in IODP Site U1308. *Marine Geology* **2009**, *258* (1–4), 60–68. https://doi.org/10.1016/j.margeo.2008.11.007.
(70) Nguyen, T.; Janik, L.; Raupach, M. Diffuse Reflectance Infrared Fourier Transform (DRIFT) Spectroscopy in Soil Studies. *Soil Res.* **1991**, 29 (1), 49. https://doi.org/10.1071/SR9910049.

Insert Table of Contents artwork here

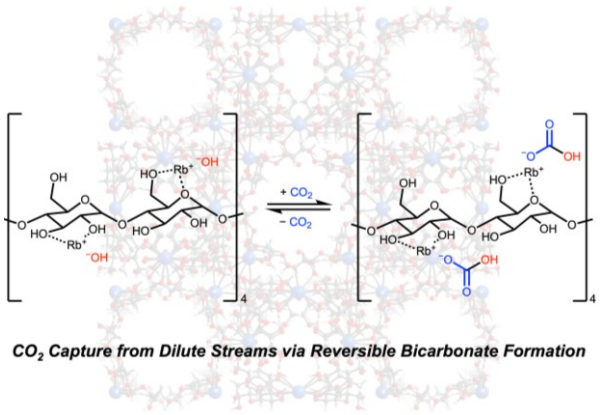

CO_2 Capture from Dilute Streams via Reversible Bicarbonate Formation